Efficiency and durability of g-C_3N_4-based coatings applied on mortar under peeling and washing trials

Yang, Yu; Ji, Tao; Yang, Zhengxian; Zhang, Yong; Su, Wenyue; Wu, Ronghan; Wu, Zehao

DOI
10.1016/j.conbuildmat.2019.117438

Publication date
2020

Document Version
Accepted author manuscript

Published in
Construction and Building Materials

Efficiency and durability of g-C_3N_4-based coatings applied on mortar under peeling and washing trials

Yu Yang[a], Tao Ji[a]*, Yong Zhang[a,b]*, Wenyue Su[c], Ronghan Wu[a], Zehao Wu[a]

[a] College of Civil Engineering, Fuzhou University, Fuzhou 350116, China

[b]Microlab, Section of Materials and Environment, Faculty of Civil Engineering and Geosciences, Delft University of Technology, 2628 CN Delft, the Netherlands

[c] State Key Laboratory of Photocatalysis on Energy and Environment, Fuzhou University, Fuzhou 350116, China

* Correspondence: jt72@fzu.edu.cn (Tao Ji), y.zhang@fzu.edu.cn (Yong Zhang), Tel.: +86 591 2286 5355, Fax: +86 591 2286 5355.

Abstract

Durability of photocatalytic coatings is a major concern in engineering practice. Here, two types of novel visible light-responsive coatings, both consisting of vinyl chloride/vinyl ester/ethylene copolymer (as a binder) and g-C_3N_4 but different in fabrication, are proposed and applied on the mortar surface. The first type is mono-layer coating (MC), where the g-C_3N_4 suspension containing the binder is directly sprayed on the mortar. The second type is double-layer coating (DC), where the binder layer is applied on mortar surface before spraying the g-C_3N_4 layer. Results show that the binder addition leads to a good anchorage of the coatings on both MC and DC mortar substrates, along with desirable resistance to peeling and washing, compared to the g-C_3N_4 coated mortar without the binder. The well-distributed binder in g-C_3N_4-based coating inevitably decreases the photocatalytic efficiency of the MC mortar due to masking effect of the binder on the coating surface. The DC mortar, on the contrary, takes full advantage of the binder adhesion by inserting a binder layer and therefore holds strong resistance to peeling and washing without compromising its photocatalytic efficiency. The proposed DC technique provides a promising strategy to fabricate highly cost-effective and durable photocatalytic coatings applied on cementitious materials.

Keywords: Durability; g-C_3N_4-based coatings; Photocatalytic NO_x removal; Mortar substrate

1. Introduction

Photocatalytic building materials, which are fabricated using photocatalyst either applied as surface coating or embedded in bulk, have been proposed for building aesthetics and environmental remediation in recent years. It is an environment-friendly process that the hole-electron pairs produced from photocatalyst under sunlight irradiation can degrade organic [1, 2] and inorganic [3, 4] contaminants as well as microorganism [5, 6] in the presence of water and oxygen. Nitrogen oxides (NO_x) are the major pollutants that strongly induce environmental problems such as urban smog, acid rains and depletion of tropospheric ozone [7, 8]. In this respect the NO_x abatement has been widely investigated in the field of photocatalytic building materials [9, 10]. It has been well demonstrated that the NO is oxidized first to NO_2 and then to HNO_3 by the light activated holes and associated active species such as superoxide ($\cdot O_2^-$) and hydroxyl radicals ($\cdot OH$) [11, 12].

In view of the publications previously reported, the titanium dioxide (TiO_2) is the most used photocatalyst in photocatalytic building materials due to its high chemical stability and relatively low price [13, 14]. Nonetheless, TiO_2 suffers from disadvantages such as low exploitation of sunlight because of its relatively large band gap (3.2 eV) [15] and fast recombination of photoinduced electron-holes [16, 17]. This to some extent impedes its application in practice. Graphitic carbon nitride (g-C_3N_4), also known as nontoxic metal-free materials, has emerged as an attractive photocatalyst with a visible-light driven bandgap (2.7 eV) and proper band edges [18, 19]. Over the past decade, g-C_3N_4 has been extensively studied for environmental pollution mitigation and renewable energy generation [20]. For instance, g-C_3N_4, typically prepared by the polycondensation of organic precursors containing both carbon and nitrogen, exhibits an effective photodegradation of organic pollutants and NO_x abatement under visible light irradiation [21, 22]. Therefore, the g-C_3N_4 could be a promising alternative photocatalyst used in building materials [23,

24].

Photocatalytic cementitious composites intermixed with TiO_2 particles for NO_x abatement have been reported previously [25, 26]. Noteworthy, most of the photocatalyst in the internal structure are difficult to participate the photo-induced reactions, leading to a high cost but low efficiency of these photocatalyst products. Photocatalytic reactions usually occur on the material surface, which is in direct contact with the sunlight and contaminants. The photocatalytic coatings prepared by spray coating [27, 28], dip-coating [29] and electrospray coating [30] have been developed to apply the uniformly dispersed photocatalyst onto the substrate surface. To date, although considerable progress on photocatalytic coatings mainly applied on stone and glass has been achieved in the recent years [31], the underlying mechanism of the coating application on stone or glass maybe not applicable to the cementitious materials due to their inherent characteristics such as high alkalinity and complex ion circumstances (Ca^{2+}, Na^{+}, OH^{-}). The research on the photocatalytic coating applied to cementitious materials is still at an infant stage, and previous reports mostly focused on optimizing photocatalytic efficiency of the photocatalytic products but that their durability in real service condition was not adequately improved [27, 32]. The durability of the coatings is a crucial concern for large-scale applications. Hassan and co-workers [33] may be the first to evaluate the durability and resistance to wear of TiO_2 surface coating applied on the concrete pavement. Since then researchers are aware of the importance to consider the durability of photocatalytic building materials and release of photocatalyst particles [34, 35]. Maury-Ramirez and co-workers [36] investigated the weathering resistance of TiO_2 coating on autoclaved aerated concrete through a dip-coating, and found a decline in TiO_2 content by more than 93% after intensive weathering. The loss of the photocatalyst from coatings caused by wearing and water flow (rainfall) results in not only a reduction of photocatalytic activity and service life [37,

65 38] but also an increase in health damage risk to humans [39, 40].

66 For immobilization of the catalyst on the substrate against rain-wash and abrasion in practical
67 service conditions, various kinds of binders including acrylic resin [41], polyethersulfone [42] and
68 fluoropolymer [43] have generally been added in these coatings. Vinyl ester is notable as additives
69 and has been widely used in coatings and adhesives with excellent resistance to a wide variety of
70 commonly encountered environments [44]. There are two main approaches for fabricating the
71 photocatalytic coatings incorporated with binder additives. First, catalyst powders are directly
72 dispersed into the binder suspension to form a homogeneous composite sol for spraying or brushing
73 process. Russa and co-workers [45, 46] were devoted to develop TiO_2 coatings for cultural heritage
74 protection and reported a nano-TiO_2 coating with desirable hydrophobicity, durability and
75 self-cleaning properties, which was prepared by brushing the acrylic water suspension mixed with
76 TiO_2. Secondly, an intermediate layer of the binder is applied on the substrate before installation of
77 the photocatalytic layer. Persico and co-workers [47] developed a multilayered transparent
78 fluoropolymeric coating applied on the quartz sheath for degradation of hydrosoluble pollutants,
79 and the perfluorinated amorphous polymer that acts as a hydrophobic primer coating can not only
80 improve the adhesion between the latter photoactive layer and the quartz, but also prevent water
81 penetration. The SiO_2 layer was applied on cement substrate before the TiO_2 layer was sprayed,
82 leading to an improved adhesion for TiO_2 coatings and a protective layer for substrate [48]. These
83 hybrid coatings, however, were developed and investigated mainly in laboratory conditions. And
84 few reports on on the resistance to wear and rain wash of these hybrid coatings applied to mortar
85 substrate is available so far [49, 50].

86 From a literature survey, little effort has been devoted to optimizing the method of binder
87 addition technique in term of efficiency and durability when preparing photoactive coating on the

mortar surface. In this work, two binder addition techniques were applied to fabricate two novel visible light-responsive coatings, composed of vinyl chloride/vinyl ester/ethylene copolymer (as a binder) and g-C_3N_4, on mortar surface. First, the binder suspension mixed with g-C_3N_4 was prayed on the mortar to form the coating. Secondly, the binder suspension is applied on mortar surface before the g-C_3N_4 suspension is sprayed. The g-C_3N_4 suspension without binder is sprayed on mortar as a control group. Under a peeling action and a simulated rain-wash process, the durability of these coated mortars was evaluated in view of g-C_3N_4 loss from the mortar surface by qualitative-quantitative SEM-EDS analysis. Hydrophobicity of these coated mortars is monitored by water contact angle measurements. The photocatalytic performances of the coated mortars were assessed in terms of NO_x removal under visible light before and after the durability tests (i.e. peeling test and washing test). This work will provide a good reference for optimizing the efficiency and durability of the mortars with photocatalytic coatings.

2. Experimental

2.1. Materials and mortar substrate

Urea was provided by Sinopharm Chemical Reagent Co. Ltd. without further purification. The binder mainly consisting of vinyl chloride/vinyl ester/ethylene copolymer (COMPAKTUNA®PRO) received from P.T.B. COMPAKTUNA was used. The characteristics of the binder are listed in Table 1. A grade of 42.5 R Portland cement (Chinese Standard) was used, taken from Anhui Conch Cement Co., Ltd. The China ISO standard sand used in the study was acquired from Xiamen ISO Standard Sand Co., Ltd. Deionized water was used throughout the experiments.

The mortar substrate was fabricated with a constant mix proportion of water: cement: sand as 0.5: 1: 3 by mass. In detail, the dry cement was mixed first with deionized water in a mixer at a low

speed for 30 s. Afterwards, sand was added into the mixture and stirred for another 90 s (low speed for 30 s and high speed for 60 s) to obtain the fresh mixtures. The fresh mortars were cast in the specific discs (Φ30 mm × 15 mm) and compacted carefully on a vibration table. Afterward, all the specimens were demolded after 24 hours, and then transferred into a curing chamber (20 °C and 98% relative humidity) for another 27 days.

Table 1

Characteristics of the binder (vinyl chloride/vinyl ester/ethylene copolymer).

Dynamic Viscosity (mPa·s)	Solid Content (%)	PH Value	Density (kg/m^3)
80~120	52 ± 1	7~9	1.1

2.2. Synthesis of g-C_3N_4

The g-C_3N_4 was prepared according to the procedures provided in previous work [51]. 10 g of urea was placed in a crucible and heated up at 550 °C for 4 h in static air with a heating rate of 3 °C min^{-1}. After cooling naturally, the resultant yellow agglomerates were milled into powders in an agate mortar for further use. The morphology and the particle size distribution of the as-prepared g-C_3N_4 are shown in Fig. 1 and Fig. 2, respectively. The particle size of the g-C_3N_4 is mostly in the range 0.06～4 μm. The BET surface area of the g-C_3N_4 is 195.3 m^2 g^{-1}.

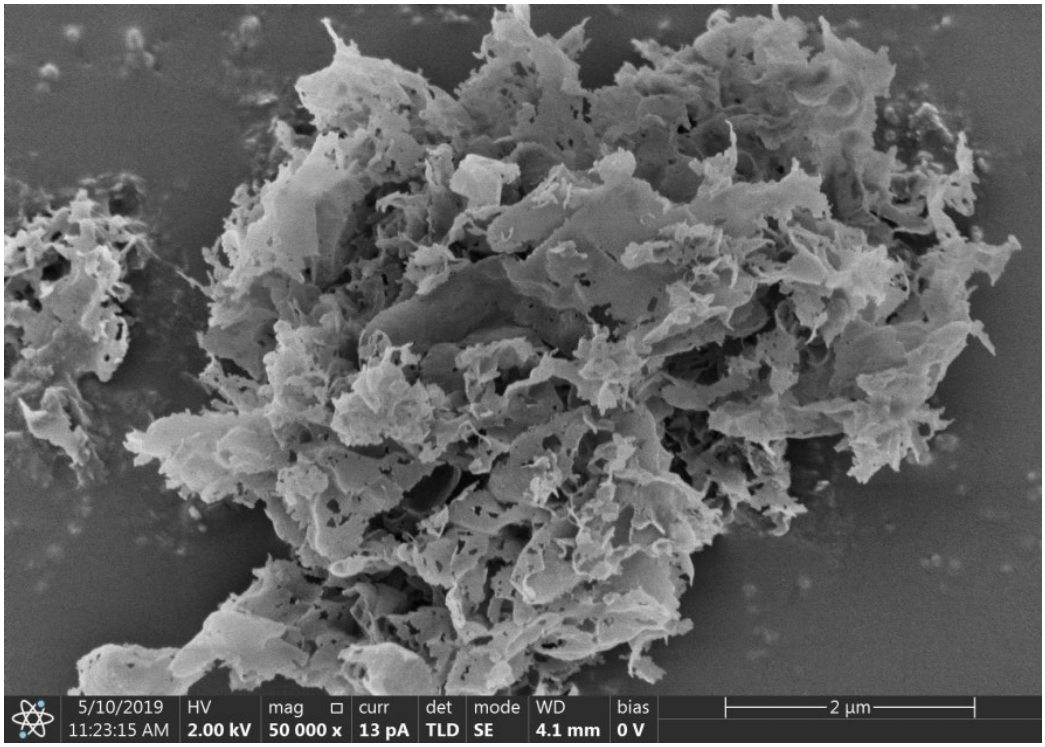

Fig. 1. Morphology of the as-prepared g-C_3N_4.

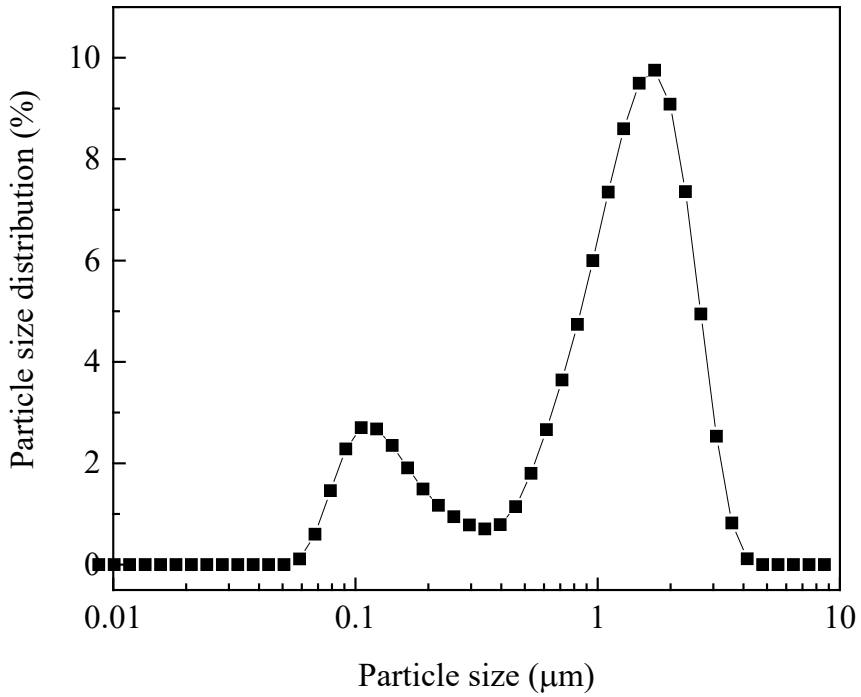

Fig. 2. Particle size distribution of the as-prepared g-C_3N_4.

133 *2.3. Coating deposition*

134 Two different procedures including mono-layer coating (MC) technique and double-layer coating
135 (DC) technique were applied on the mortar to prepare the g-C_3N_4-based coatings. A diagram for
136 illustrating the preparation process is shown in Fig. 3. In detail, the binder was completely dissolved
137 in deionized water via vigorously stirring at room temperature for 1 hour and became a
138 homogeneous binder suspension (1 wt %). The g-C_3N_4 suspensions A and B (15 g L^{-1}) were
139 obtained via 2 hours' sonication of the g-C_3N_4 powders in deionized water and in the binder
140 suspension, respectively. The g-C_3N_4 suspension B was directly sprayed on the mortar to a
141 monolayered g-C_3N_4-based coating mortar, denoted as MCM. To prepare the mortar coated with
142 double-layered g-C_3N_4-based coatings, the binder suspension was first sprayed on the surface of
143 mortar, and then dried at ambient temperature for 3 min before spraying the g-C_3N_4 suspension A,
144 denoted as DCM (double-layer g-C_3N_4-based coating mortar). For both MCM and DCM,
145 approximately 0.7 mg cm^{-2} of binder was applied on each sample. In addition, the g-C_3N_4
146 suspension A was sprayed on the mortar as a control sample. After coating, the coated mortars were
147 dried for 24 h in a controlled laboratory environment (25 ± 2 ℃ and 30 ± 5% RH) and stored in
148 dark conditions. For all the coated mortars, approximately 1.0 mg cm^{-2} of g-C_3N_4 was applied.

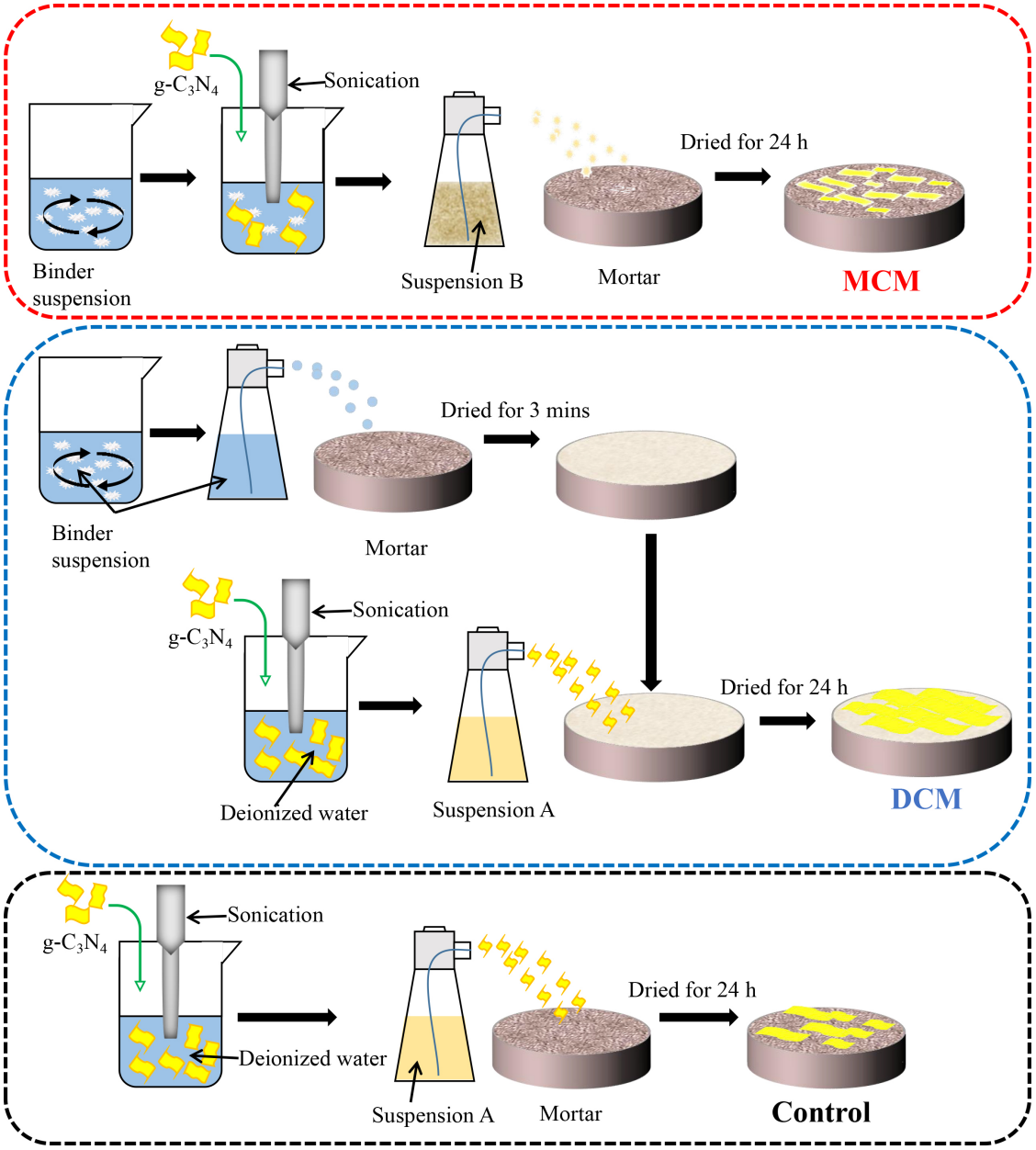

Fig. 3. Schematic illustration on the preparation of the coated mortars.

2.4. Durability tests

The durability of the coated mortars was evaluated via peeling test and water wash process. The peeling experiment was performed according to a method reported previously, which was used for evaluating the surface cohesion of mortars and stones [52, 53]. In a typical process, a commercial adhesive tape (M&G Chenguang Stationery co., Ltd.) was stuck to the surface of the coated mortar and smoothed with gentle finger pressure; after 10 seconds, the tape was removed rapidly. The test

for each sample was repeated for a couple of times preassigned. New strips were used for each time.

The rain wash is the most ubiquitous deterioration factor affecting the whole building facades and it is a primary concern for the durability of the coated mortar in real service conditions. The rain-wash process was simulated in this work (Fig. 4), the coated mortars were immersed in deionized water with an ultrasonication, using a Shu Mei ultrasonic bath (KQ-200KDB, 40 kHz, 200 W). After the ultrasonication for prescribed times, the samples were washed with deionized water and oven dried at 60 °C.

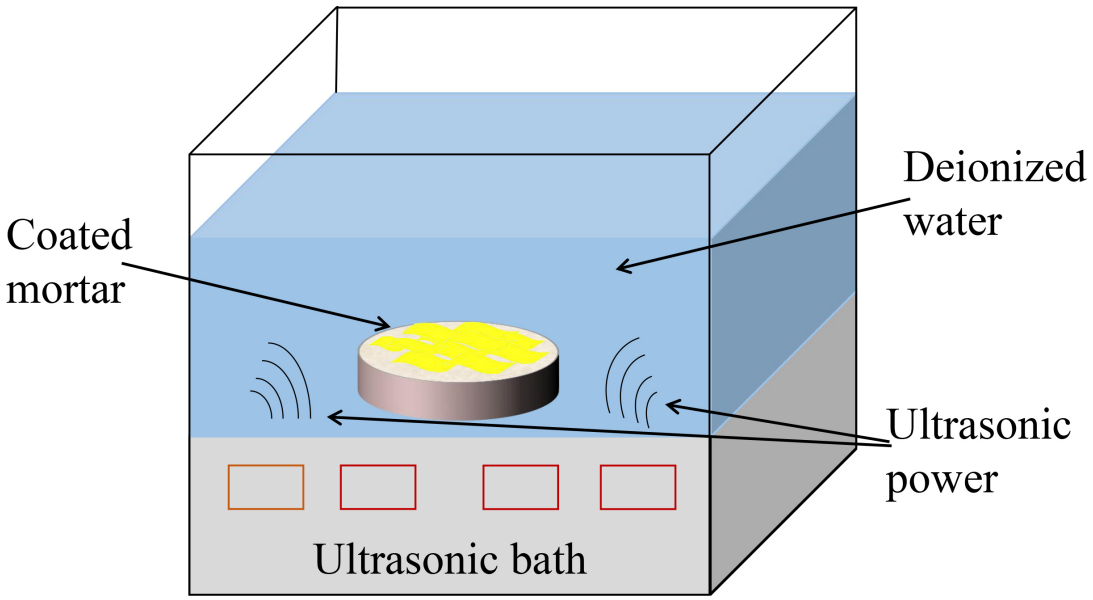

Fig. 4. Sketch of the experimental setup for the coated mortars under simulated rain-wash.

2.5. SEM-EDS analyses

Scanning Electron Microscopy (SEM) equipped with Energy-dispersive X-ray spectroscopy (EDS) (Bruker Quanta 250) was used to observe the morphology of the coatings on the mortars and to investigate the distribution of Nitrogen (noted as N hereafter) on the mortar surface. Comparative SEM observations and quantitative analyses of N by EDS were performed before and after the durability tests, to study the effect of the peeling action and the rain-wash process on the coated mortar. Morphological and elemental analyses were performed at an accelerated voltage of 15 kV.

Distribution maps of element were acquired in Live Spectrum Mapping mode. The analytic time was 10 min for each EDS scan.

2.6. Contact angle measurements

Water contact angle (WCA) of the coated mortars was measured in order to evaluate the hydrophobicity of the coatings before and after the durability tests and after exposure to light/dark. A contact angle meter (OCA20, Dataphysics) was used to measure the WCAs. A water droplet (5 μL) was gently placed on the surface of the coated mortars using a microsyringe. Five locations on the coatings were chosen to measure the WCA and these were then averaged to report the equilibrium contact angle.

2.7. Photocatalytic NO_x removal test

The capability in air purification of the coated mortars was evaluated by photocatalytic NO_x abatement in a continuous reactor under visible light irradiation, based on a regular photocatalytic procedure ISO/DIS 22197-1. The schematic diagram of NO_x removal experimental set-up is shown in Fig. 5. The NO gas was supplied from a gas container with 6 ppm NO concentration (N_2 balance). The air was provided from a compressed cylinder. The targeted concentration (1 ± 0.05 ppm NO) of the testing gas was achieved by mixing air stream and NO gas using the gas mass flow meters. The flow rate of the targeted gas was adjusted to 0.6 L min^{-1}, and its relative humidity was kept at 50% by passing the air streams through a water bubbler. The coated mortar was put in the middle of the cylindrical reactor (Φ60 mm × 50 mm), which was made of glass and covered with quartz glass window. A 300 W xenon lamp with a light passing through a UV cut off filter (λ>420 nm) was vertically placed outside the reactor as a light source. The accurate measurement of the

concentration of NO, NO_x and NO_2 was carried out using a chemiluminescence analyzer (Model 42i, Thermo Environmental Instruments Inc). For each test, the targeted gas (1 ppm NO) was passed over the coated mortars in the dark for a period of 30 min before the irradiation. The irradiation experiments were carried out for another 30 min. Each test was repeated three times to obtain an average value. The amount of NO_x abatement was expressed as a subtraction of the NO_2 generated from the NO removed according to previous reports [26, 54]. The calculation of the amount of NO_x abatement is shown below:

$$Q_{NO_x} = \left(\frac{f}{22.4}\right)\left\{\int([NO]_0 - [NO])dt - \int([NO_2] - [NO_2]_0)dt\right\}/(A \times T) \quad (1)$$

where Q_{NO_x} (μmol m^{-2} h^{-1}) is the amount of NO_x abatement; $[NO]_0$ and $[NO_2]_0$ (ppm) are the initial concentration of the nitrogen monoxide and the nitrogen dioxide, respectively; [NO] and $[NO_2]$ (ppm) are the concentration of the nitrogen monoxide and the nitrogen dioxide, respectively, under visible light irradiation; t (min) is the time of removal operation; f (L min^{-1}) is the flow rate at the standard state (273K, 1.013 kPa); A (m^2) is the surface area of the coated mortar; T (30 min for all experiments) is the duration of the photocatalytic process; 22.4 represents that the volume of 1 mol ideal gas at the standard state is 22.4 L (ideal gas law).

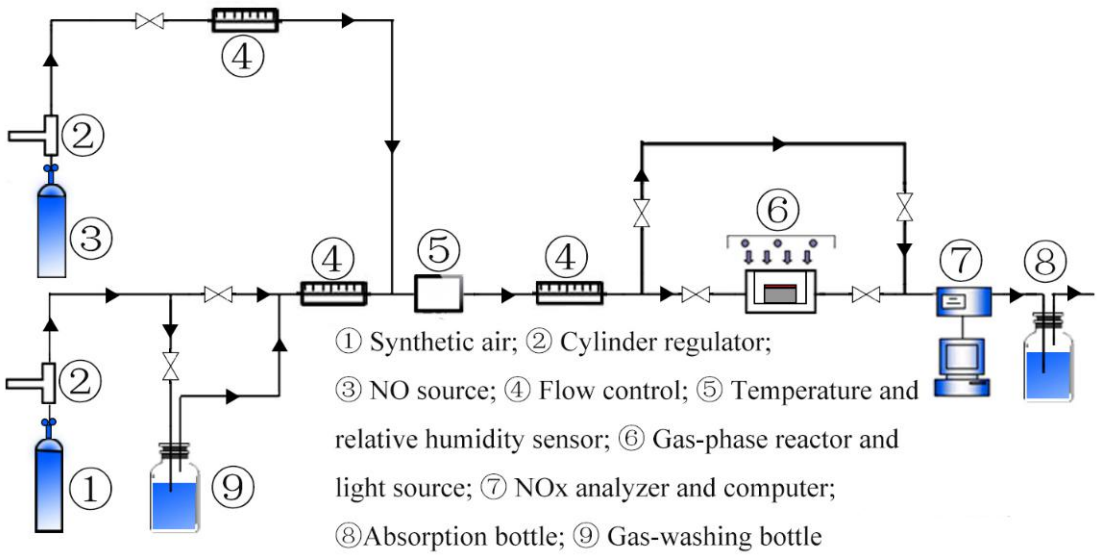

Fig. 5. Schematic diagram of NO_x removal experimental set-up [23].

3. Results and discussion

3.1. *Microscopic observations*

Fig. 6 shows the microstructure of the coated mortars before the durability tests. The g-C_3N_4-based coatings can be observed clearly on all the samples, and mask the original surface morphology of the mortars. These coatings are consistent with EDS distribution maps where abundant C and N can be detected (Figs. S1, S2 and S3). The abundant cracks with raised edges can be observed on the control (Fig. 6a). The obvious gaps between the mortar substrate and the coatings can also be found in the cross-sectional images (Fig. 6d), suggesting a low anchorage of the coating to the mortar substrate. This can be explained by the fact that the g-C_3N_4 particles adhere to each other more strongly than their adhesion to the mortar substrate due to the high surface energy of the g-C_3N_4 particle. The MCM shows a smooth surface without visible crack (Fig. 6b). This is attributed to the bonding effect of the intermixed binders between the g-C_3N_4 particles. Meanwhile, thanks to the adhesion of the binders, the coatings are attached tightly onto the mortars (Fig. 6e), presenting a good anchorage of the coatings to the mortar substrate. At higher magnifications (Figs. 7a and 7b), it is obvious that the g-C_3N_4 particles were covered by the amorphous binders compared to the identifiable g-C_3N_4 particles on the control. This corresponds well with the uniform distribution of Cl in the coatings (Fig. S2). For the DCM (Fig. 6c), the size of the micro cracks is smaller than that on the control, but larger than that on the MCM. This can be ascribed to the different distribution of the binders in the two samples. Compared to the uniformly distributed binders in the g-C_3N_4 layer (MCM), the insertion layer of the binders in the DCM only provided an anchoring effect for the bottom of the g-C_3N_4 layer. Hence, the cohesion of g-C_3N_4 particles still cause a few cracks on the g-C_3N_4 layer. Compared to the control with observable

rough mortar substrate in the cracks, the smooth surface composed of binders is observed in the bottom of the micro cracks. This is in coincidence with the distribution of Cl on the surface of DCM (Fig. S3). Additionally, the coatings on the DCM are stuck closely on the substrates, showing a good anchorage on the mortar surface. In the cross-sectional images (Fig. 6f), the compatible binders attached compactly on the mortar were in close contact with the g-C_3N_4 layer, displaying a good bond between the g-C_3N_4 layer and the mortar substrate.

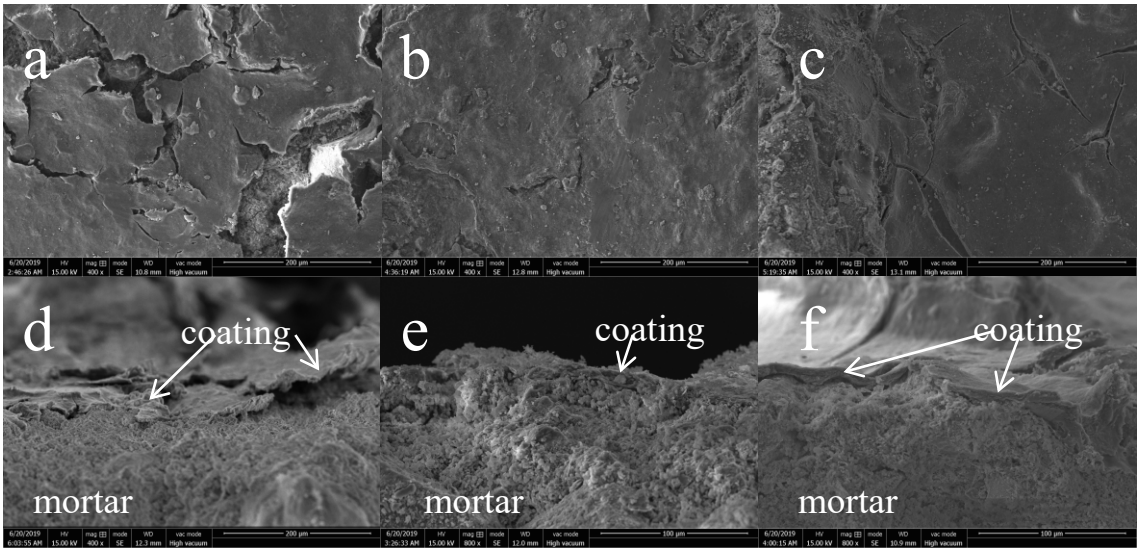

Fig. 6. Morphologies of the coated mortar surfaces and cross sections: (a) and (d) control; (b) and (e) MCM; (c) and (f) DCM.

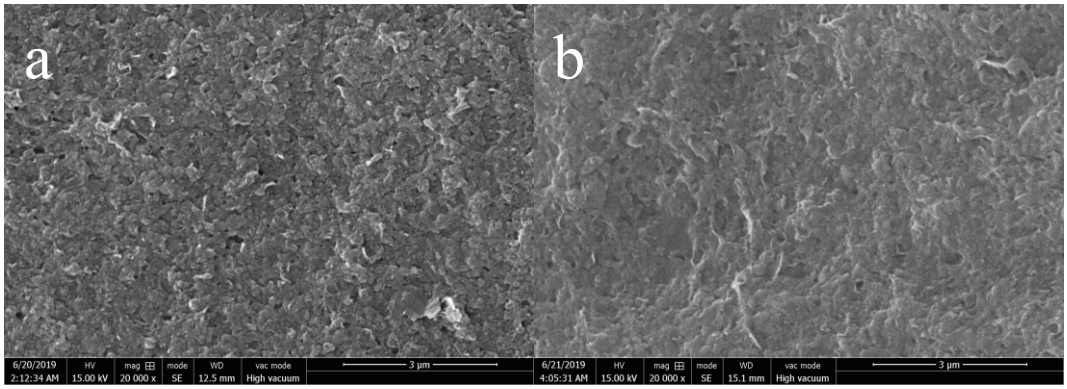

Fig. 7. Surface morphologies of (a) control and (b) MCM at high magnifications.

Fig. 8 shows the surface morphology of the control, MCM and DCM after 5 times of peeling

action. For the control, the peeling action results in a large removal of the fissured coatings, leaving a rough surface morphology of the mortars and indicating a weak resistance to human touch. This can be attributed to the low adhesion of the mortar substrate. The MCM exhibits some rough mortar surface after peeling, while most coatings remained on the surface due to the improved adhesion from the intermixed binders. It has been reported that the intermixed binders can improve the wearing resistance and stability of the coatings on the substrate [55]. For the DCM, a good stability of the coatings is found under the peeling impact test. The surface morphology is almost unchanged after peeling in spite of a little exfoliation of the g-C_3N_4 layer, indicating a strong resistance to peeling. This can be attributed to the strengthened bonding effect provided by the binder layer between the mortar substrate and the g-C_3N_4 layer.

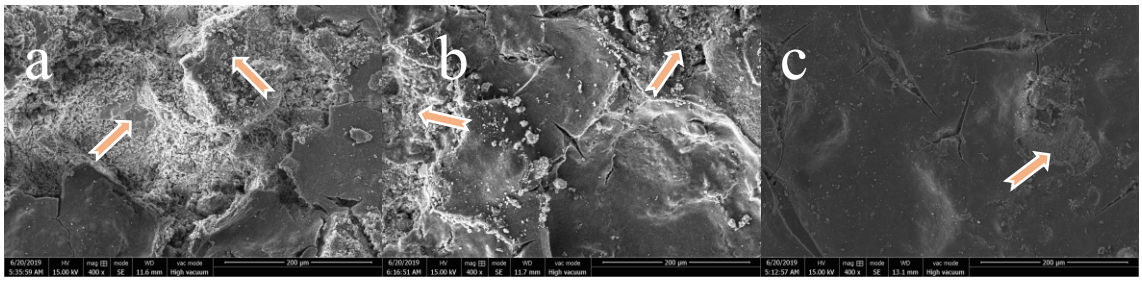

Fig. 8. Surface morphologies of (a) control; (b) MCM and (c) DCM after peeling.

Fig. 9 shows the microscopic morphologies for the control, MCM and DCM after 60 min washing. The control exhibits extensive rough surface of mortar substrate with few fragment of g-C_3N_4 layer (Fig. 9a), indicating that the water washing has a severe impact on the coatings of the control, almost a complete loss of the coating. These findings demonstrate that the direct application of photocatalyst particles onto the mortar is not effective due to the weak resistance to washing and peeling. For the MCM, the larger area of g-C_3N_4 layer remained after washing compared to that on the control. This is attributed to the bonding effect of the intermixed binders, resulting in a better resistance to washing. It should be pointed out that the bonding effect of the intermixed binders in

this MCM is limited due to the relatively low amount of intermixed binder. As a result, the CNNs coatings on the MCM were partially removed from the surface, leaving rough mortar surface when subjected to the simulated rain wash (Fig. 9b). As for the DCM, most g-C_3N_4 layers were still attached on the surface after washing, demonstrating a strong washing resistance. This can be attributed to the strong adhesion provided by binder layer. It is noteworthy that the larger cracks can be seen on the DCM after washing, suggesting that the main loss of g-C_3N_4 occurs at the discontinuous coating edge. The study on further optimization of the durability of the coated mortars is in progress to improve the continuity of the coating on the mortar.

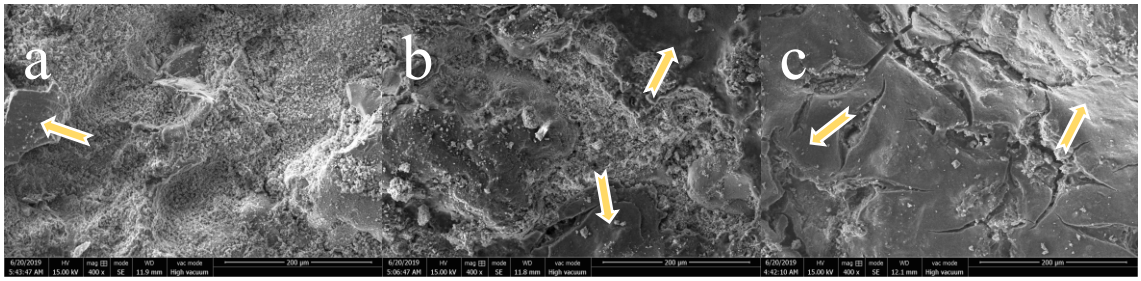

Fig. 9. Surface morphologies of (a) control; (b) MCM and (c) DCM after washing.

In order to further investigate the effect of peeling and washing on the coated mortars, the EDS analysis was used to check the N content in the coatings before and after the durability tests. The N signal can be regarded as coming from g-C_3N_4 attached on the surface of the coated mortar, and the N content measured on the surface of the coated mortars are reported in Table 2. The content of N recorded on the surface of coated mortars after the washing trial was remarkably lower than that after the peeling trial. Accordingly, the washing trial has a larger deterioration impact than the peeling trial. As expected, the control exhibits the lowest N content after peeling and washing, which is reduced by 59% and 79%, respectively. Due to the adhesion of the intermixed binders, the reduction of the N content on the MCM was smaller, 26% and 29 % respectively, than that of the control after peeling and washing. Meanwhile the remaining N content of MCM, which is higher

than that of the control, drops from approximately 39.3% to 29.1% and 16.2%, corresponding to peeling test and washing test, respectively. More importantly, the DCM shows the least reduction in the N content after peeling and washing, about 15% and 21% respectively, and remains the highest content of N compared to the MCM and the control, indicating the strongest resistance to peeling and washing. As mentioned above, different binder addition techniques have dramatically different effects on the durability of the coatings. Compared to the intermixed binder in the coating, a prior layer of binder contributes to the stronger resistance to coating exfoliation under peeling and washing trials.

Table 2

N content measured on the mortar surface (%).

	Before Durability tests	After 5 times of peeling	Δ	After 60 min of washing	Δ
Control	44.4 ± 5.4	18.1 ± 3.5	-59%	9.5 ± 2.2	-79%
MCM	39.3 ± 6.8	29.1 ± 6.3	-26%	16.2 ± 3.4	-59%
DCM	43.4 ± 4.6	37.1 ± 8.6	-15%	34.5 ± 6.7	-21%

3.2. Contact angle measurements

The wetting property of the coated mortars was investigated by the water contact angle (WCA) measurements. The results for MCM and DCM before and after durability tests are listed in Table 3. The WCA for the control cannot be detected, owing to the strong capillary water absorption of the mortar substrate and the fragmented g-C_3N_4 layer (Fig. 6a). Before the durability tests the WCA values of both MCM and DCM are higher than 80°, indicating an improved resistance to

312 water penetration due to the inherent hydrophobic behaviour of the binder. This is favourable for
313 protecting the substrate from aggressive environmental hazards. After the durability tests, the WCA
314 values of both MCM and DCM decrease slightly after the exfoliation of coatings, and the tested
315 WCA value of DCM is clearly higher than that of MCM. This corresponds well with the removal of
316 the coatings observed on the mortar surface (Figs. 8 and 9). The change of the WCA after exposure
317 to light/dark is further monitored. The results are shown in Fig. 10. After 4 hours of irradiation, the
318 WCA value of MCM and DCM drastically decreases to 18.7° and 8.7 ± 5°, respectively, both
319 exhibiting a hydrophilic surface. This can be attributed to the increase in hydroxyl-group
320 concentration on the surface of the g-C_3N_4 in the presence of water molecules under light irradiation.
321 It was reported [56] that the hydrophilicity induced by the photocatalyst under solar radiation can be
322 responsible for the decrease in the contact angles in the mixture coatings. After keeping the sample
323 in dark for 12 hours, the WCA value increases again, reaching 63.4 ± 10° and 67.2 ± 12° for DCM
324 and MCM, respectively. This can be explained by the fact that the hydroxyl groups are slowly
325 replaced by atmospheric oxygen [57].
326
327 **Table 3**
328 Water contact angles of the coated mortars (°).

	Before durability tests	After 5 times of peeling	After 60 min of washing
Control	0	-	-
MCM	80.9 ± 3	70.3 ± 5	61.0 ± 6
DCM	83.1 ± 2	75.5 ± 6	70.1 ± 6

329

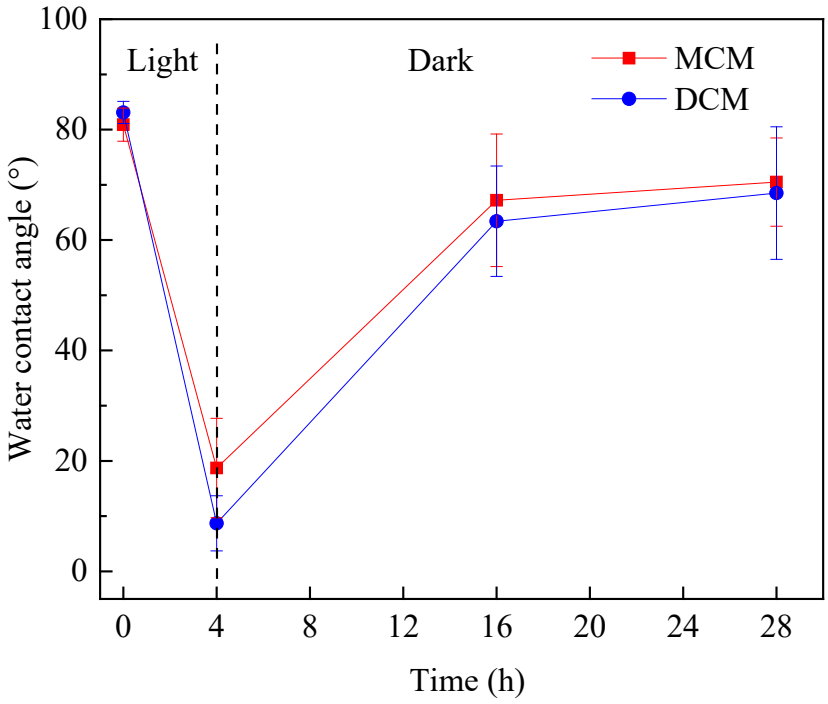

Fig. 10. Change of WCA with exposure to light/dark.

3.3. Photocatalytic activity of the coated mortars

The photocatalytic performance of the coated mortars before and after subjecting to various degrees of peeling and washing is shown in Figs. 11 and 12, respectively. Table 4 presents the loss rate of the NO_x removal efficiency of the coated mortars after 5 times of peeling and 60 min of washing. Before these durability tests, all the coated mortars show a highly efficient NO_x removal under visible light irradiation. This is reasonable given that the active species ($\cdot O_2^-$ and $\cdot OH$) formed on the g-C_3N_4 can oxidize NO_x to NO_3^- [58]. Among the three samples, the DCM presents the highest photocatalytic NO_x removal efficiency (283.9 μmol m^{-2} h^{-1}) than the control and the MCM. The MCM exhibits the lowest photocatalytic NO_x removal efficiency (230.8 μmol m^{-2} h^{-1}), caused by coverage of the g-C_3N_4 by the binders. This respect is evidently supported by the observations from SEM image (Fig. 7). The masking effect of the binders becomes pronounced

with an increasing content of the binders due to the higher probability of g-C_3N_4 covered by binders, resulting in a remarkable decrease in the NO_x removal efficiency of MCM (see Fig. S4). This is in good agreement with the findings reported previously [59].

Table 4

Loss rate of the NO_x removal efficiency of the coated mortars after 5 times of peeling and 60 min of washing (%).

	After 5 times of peeling	After 60 min of washing
Control	56.8%	81.9%
MCM	34.1%	55.3%
DCM	18.1%	28.8%

As shown in Fig. 11, with the increased times of peeling, the photocatalytic NO_x removal efficiency of all the coated mortars shows a decreasing trend. The control exhibits the largest decline about 56.8% compared to the MCM and DCM after 5 times of peeling action. This corresponds well with the large loss of g-C_3N_4 on the mortar surface due to the weak adhesion of the mortar substrate (Table 2). After 5 times of peeling action, the photocatalytic NO_x removal efficiency of the MCM is about 152.1 μmol m^{-2} h^{-1}, which is 33.3% higher that of the control (114.1 μmol m^{-2} h^{-1}). This is attributed to the fact that the intermixed binders are able to help preserve g-C_3N_4 particles on the surface. As for the DCM, the peeling action causes the least loss of photocatalytic performance (18.1%), dropping from 283.9 μmol m^{-2} h^{-1} to 232.5 μmol m^{-2} h^{-1}. After 5 times of peeling action the DCM presents the highest photocatalytic NO_x removal efficiency, which is 2.0 times and 1.5 times higher than that of the control and the MCM, respectively. These

results coincide well with the observed microscopic morphology and N content on the mortar surface.

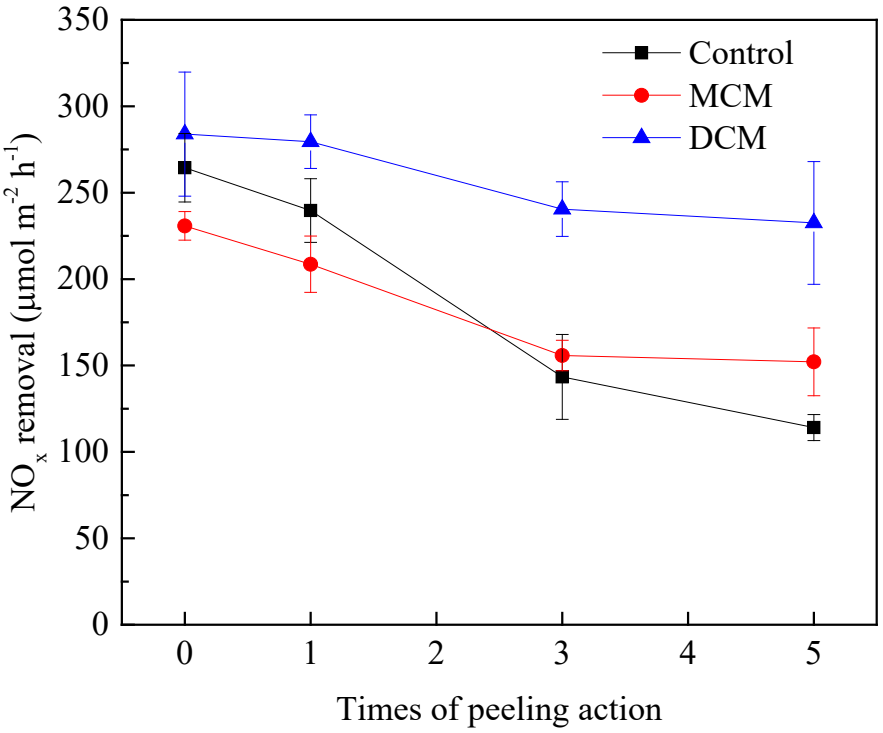

Fig. 11. Photocatalytic NO_x removal efficiency of the coated mortars subjected to peeling action.

The photocatalytic NO_x removal efficiency has decreased for all the coated mortars after exposure to the washing trials, as shown in Fig. 12. With the increase of the washing time from 20 min to 60 min, a further decreasing trend of the photocatalytic NO_x removal efficiency is observed for all the samples. The control suffers an enormous reduction of about 81.9% in the NO_x removal efficiency after 60 min of washing, falling from 264.4 μmol m^{-2} h^{-1} to 47.8 μmol m^{-2} h^{-1}, suggesting a fragile resistance to washing. It is reasonable to consider that application of the photocatalyst without additives on the actual building surfaces is impracticable due to its week stability of coatings and low long-term photocatalytic performance. For the MCM, distribution of the binder in the coatings can help to improve the bonding between g-C_3N_4 and mortar substrate. After 60 min of

377 washing the MCM shows a NO_x removal efficiency of 103.2 μmol m^{-2} h^{-1}, which is 2.1 times higher
378 than that of the control. It is worth noting that the DCM exhibits the lowest loss of NO_x removal
379 efficiency of about 28.8% compared to the MCM and the control when subjected to 60 min of
380 washing action. In contrast, the DCM retains the highest NO_x removal efficiency of 202.1 μmol m^{-2}
381 h^{-1}, which is in line with the highest N content observed above (Table 2), and it is 1.9 times and 4.2
382 times higher than that of the control and the MCM, respectively. Hence, a coating approach at
383 which the highest NO_x removal efficiency of the coated mortars after peeling and washing are
384 achieved is optimized. Furthermore, the relationship between photocatalytic NO_x removal
385 efficiency and N content on the mortar surface is established, as shown in Fig. 13. It can be
386 observed that a linear relationship exists between the NO_x removal efficiency and the N content,
387 with a regression coefficient R^2 of 0.987.
388

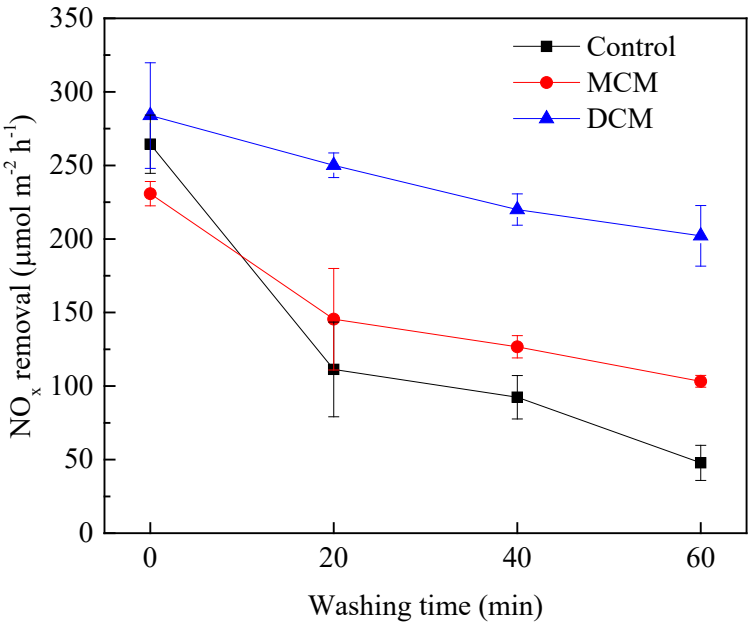

389

390 Fig. 12. Photocatalytic NO_x removal efficiency of the coated mortars versus washing time.

391

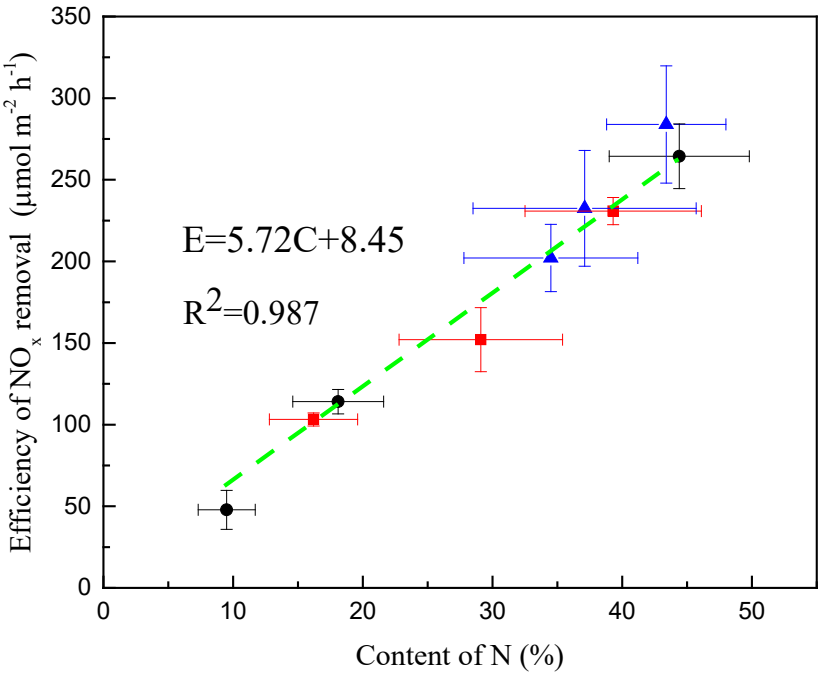

392

393 Fig. 13. Relationship between photocatalytic NO_x removal efficiency and N content on the mortar

394 surface.

395

396 **4. Discussion**

397 Application of photocatalyst as coating on the outdoor exposed building materials has been

398 intensively developed for self-cleaning and depollution [60, 61]. Incorporation of the binder with

399 photocatalyst, a type of hybrid coating, is an often-adopted approach to guarantee the long-term

400 property of the photocatalytic coating in real service condition. [45, 56]. However, few reports on

401 the durability of the hybrid coating applied to mortar substrates are available, and little effort has

402 been devoted to optimizing the binder addition technique in term of efficiency and durability when

403 preparing photoactive coating on the mortar surface. In this work, two binder addition techniques

404 have been successfully applied to fabricate novel visible light-responsive coatings, composed of

405 vinyl chloride/vinyl ester/ethylene copolymer and g-C_3N_4, on mortar surface. Their photocatalytic

406 NO_x removal efficiency and resistance to peeling and washing are investigated and compared in
407 detail.

408 Based on the above results, the influence of different approaches of binder addition on the
409 photocatalytic activity and durability of the coated mortars is illustrated in Fig. 14. For the MCM,
410 the intermixed binders are almost uniformly distributed in the g-C_3N_4-based layer. The binders
411 distributed on the upper surface of the coatings are detrimental to the photocatalytic activity due to
412 its masking effect that drastically weakens the contact of the g-C_3N_4 with the NO_x. The lowest NO_x
413 removal efficiency before the durability tests is consequently presented in the MCM compared with
414 the control and the DCM. Due to the drying shrinkage, the control exhibits discontinuous coatings
415 with large cracks, leading to a reduction in surface areas of the g-C_3N_4 coatings. This is detrimental
416 to the photocatalytic reaction. While the DCM presents smooth coatings with smaller crack due to
417 the good adhesion provided by the pre-inserted binder layer. As a result, the initial photocatalytic
418 NO_x removal efficiency of the DCM is higher than that of the control.

419 Previous studies [53, 62] on durability of TiO_2 coatings applied on different substrates have
420 shown the high surface roughness of substrate along with good durability of the photoactive coating
421 due to the favourable adhesion of the substrate. Nonetheless, the aggressive peeling and washing
422 actions can cause a significant loss of g-C_3N_4 layer on the control in spite of its sufficiently rough
423 surface. This demonstrates that the surface roughness of substrate holds limited role on the
424 durability of the coatings against the mechanical effects of human touch and real rain, and the direct
425 application of photocatalyst particles onto the mortar is inadvisable due to their poor durability.

426 For the MCM, the binders on the bottom of the coatings can contribute to the bonding effect
427 between the mortar and the g-C_3N_4-based layer, resulting in a good resistance to peeling and
428 washing. It is reasonable to consider that a bigger amount of binders on the bottom of the coatings,

from the MCM with a larger content of binders, can provide more bonds between the mortar and the g-C_3N_4-based layer. However, the increased content of the intermixed binders tends to cause a reasonable increase in the amount of binders on the upper surface of the coatings, resulting in a decline in the photocatalytic performance. It can then be deduced that the MCM with the stronger resistance to coating exfoliation under peeling and washing trials holds inevitably the lower photocatalytic efficiency. This partly impedes its large-scale application due to high cost and low efficiency.

As for the DCM, the double-layer structure takes full advantage of binder adhesion by employing an intermediate binder layer before construction of the g-C_3N_4 layer. The binder layer can provide sufficient adhesion for the g-C_3N_4 layer without compromising its photocatalytic efficiency, resulting in strong resistance to peeling and washing. What's more, the dosage of the binder layer can be increased to acquire desirable bonds between the mortar substrate and the g-C_3N_4 layer without any adverse impact on its photocatalytic activity. The proposed double-layer coating technique, which overcomes the contradiction between durability and efficiency often in the conventional mono-layer coating, is proved to fabricate durable photocatalytic coating on cementitious materials without compromising its photocatalytic efficiency. It should be pointed out that the intermediate binder layer only contributes to bonding effect on the bottom of the g-C_3N_4 layer. A few cracks occur accordingly on the surface of the g-C_3N_4 layer, which will be troubles potentially for loss of the coatings when subjected to the action of the peeling and washing. Improvements on the coating for uniformity without cracking to achieve better durability will be the subject of a further study.

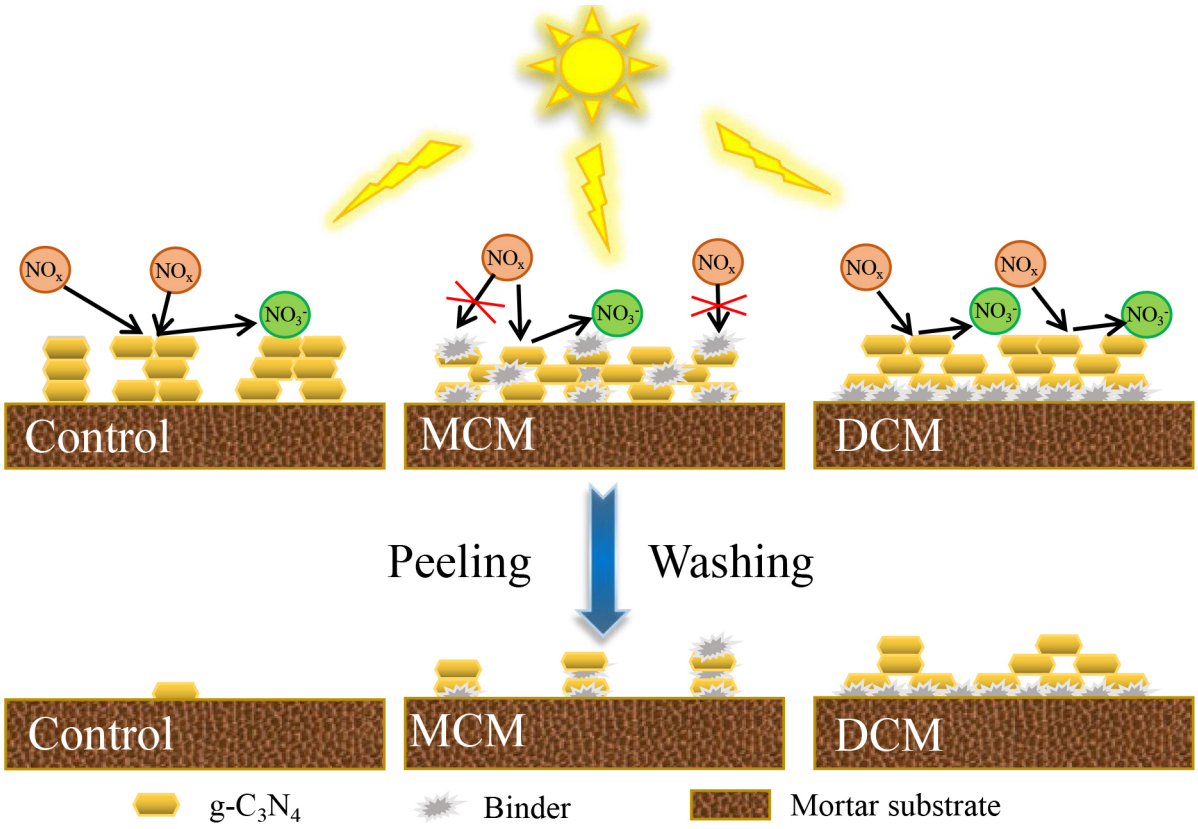

Fig. 14. Schematic illustration of the photocatalytic activity and durability of the coated mortars fabricated by different approaches.

The primary objective of this article is to propose preliminary strategy to fabricate highly cost-effective and durable photocatalytic coatings applied on cementitious materials, and provide the information on the mechanical resistance to peeling and washing of these coatings. The durability assessment on surface carbonation and aging of the proposed double-layer coating applied on cementitious materials is worthwhile to continue in detail for further study. The carbonation of cementitious materials is a universal phenomenon, where the formation of calcite via chemical reaction between calcium hydroxide in the cement paste and carbon dioxide (CO_2) from the air can block the surface of the catalyst [63]. The binder acts as a barrier that can sufficiently prevent the contact between the mortar surface and the CO_2 in the air. The binder in MC is usually randomly distributed and can be relatively poorly connected. The binder in DC, in contrast, is

present as a whole on the mortar surface and is therefore well connected, as already illustrated in Fig. 14. In this sense, the resistance to CO_2 ingress of the DC should be stronger than that of the MC. Moreover, in the field of photocatalytic coatings, special effort should be paid to the well-known issue that polymeric binder can be degraded in the process of photocatalysis. The photocatalysis occurs primarily on the surface of the coating which is accessible to the light. In the MC, the oxidative species ($\cdot O_2^-$ and $\cdot OH$) formed on the surface are prone to degrade the binder around the surface. As for the DC, the oxidative species need to pass through the g-C_3N_4 layer to degrade the binder layer. In this penetration process, the oxidative species may be partly consumed. What's more, the g-C_3N_4 layer provides a shield for the binder layer to protect against UV radiation. As a consequence, the resistance of DC to aging can be stronger than that of MC. Also, by increasing the thickness of g-C_3N_4 layer in the coating, the photo-induced degradation of the binder layer can reasonably be decreased. Besides, nitrate ion or nitric acid is usually considered as the inert end product of the NO_x photocatalytic degradation. And the accumulated nitrate ion or nitric acid often stays on the surface of photocatalyst until it is eventually washed off by rainfall. It is noteworthy that the effect of nitrate ion or nitric acid on the photoactivity of catalyst remains controversial. Paolini and co-workers [64] discovered an unexpected increase in anatase near infrared (NIR) reflectance but a decrease in photocatalytic activity during environmental exposure, which can be attributed to the nitric acid generated by the degradation of NO_x causes partial reduction in crystallinity of TiO_2. Che and co-workers [65] found that after stirring in HNO_3 solution, the photocatalytic performance of graphitic carbon nitride was significantly enhanced by intercalated hydrogen bond effect of NO_3^-. Yet, it is also reported that the accumulated nitrate ion on the photocatalyst surface could easily occupy the active sites, which is partially detrimental to the photocatalytic activity [66]. The effect of nitrate ion and nitric acid on the long-term photoactivity

shall be consequently considered in future investigation. A more detailed and complete experimental study is in the stage of development to provide a solid validation for the more durable behaviors of the DC when used in real engineering practice.

5. Conclusions

Two novel visible light-responsive coatings composed of vinyl chloride/vinyl ester/ethylene copolymer and g-C_3N_4, which are applied on mortar surface, have been developed by two binder addition techniques including mono-layer coating (MC) technique and double-layer coating (DC) technique, respectively. The g-C_3N_4 suspension without binder is sprayed on mortar as a control group. The coated mortars hold efficient NO_x removal efficiency under visible light irradiation and desirable hydrophobicity. Major findings can be summarized below:

(1) In spite of high surface roughness of mortar, the control exhibits discontinuous coatings with large crack due to the drying shrinkage, showing a low anchorage to mortar substrate. This can be responsible for the week resistance to peeling and washing.

(2) Compared to the control, the MC and DC mortars present a better anchorage to mortar substrate due to the adhesion of the binder, along with a better resistance to peeling and washing. The addition of binder accounts for the hydrophobicity of MC and DC mortars.

(3) Before the durability tests (i.e. peeling test and washing test), the MC mortar exhibits the lowest photocatalytic efficiency compared to both the control and the DC mortar due to the masking effect of the intermixed binder, and the MC mortar with higher amount of binder has the lower photocatalytic efficiency, which impedes its practical application due to the high cost and low effectiveness.

(4) Contradiction between durability and efficiency often exists in the conventional MC. The

proposed DC technique, which overcomes that contradiction, is proved to fabricate durable photocatalytic coating on cementitious materials without compromising its photocatalytic efficiency.

Acknowledgement

This work was supported by the National Natural Science Foundation of China (Grant No. 51878179).

References

[1] A. Calia, M. Lettieri, M. Masieri, S. Pal, A. Licciulli, V. Arima, Limestones coated with photocatalytic TiO2 to enhance building surface with self-cleaning and depolluting abilities, Journal of cleaner production 165 (2017) 1036-1047.

[2] T. Adachi, S.S. Latthe, S.W. Gosavi, N. Roy, N. Suzuki, H. Ikari, K. Kato, K.-i. Katsumata, K. Nakata, M. Furudate, Photocatalytic, superhydrophilic, self-cleaning TiO2 coating on cheap, light-weight, flexible polycarbonate substrates, Applied Surface Science 458 (2018) 917-923.

[3] E. Boonen, A. Beeldens, I. Dirkx, V. Bams, Durability of cementitious photocatalytic building materials, Catalysis Today 287 (2017) 196-202.

[4] M.-Z. Guo, C.S. Poon, Superior photocatalytic NOx removal of cementitious materials prepared with white cement over ordinary Portland cement and the underlying mechanisms, Cement and Concrete Composites 90 (2018) 42-49.

[5] S. Veltri, A.M. Palermo, G. De Filpo, F. Xu, Subsurface treatment of TiO2 nanoparticles for limestone: Prolonged surface photocatalytic biocidal activities, Building and Environment 149 (2019) 655-661.

[6] G.B. Goffredo, S. Accoroni, C. Totti, T. Romagnoli, L. Valentini, P. Munafo, Titanium dioxide based nanotreatments to inhibit microalgal fouling on building stone surfaces, Building and Environment 112 (2017) 209-222.

[7] J. de OB Lira, N. Padoin, V.J. Vilar, C. Soares, Photocatalytic NOx abatement: Mathematical modeling, CFD validation and reactor analysis, Journal of hazardous materials 372 (2019) 145-153.

[8] J. Lasek, Y.-H. Yu, J.C. Wu, Removal of NOx by photocatalytic processes, Journal of Photochemistry and Photobiology C: Photochemistry Reviews 14 (2013) 29-52.

[9] M. Pérez-Nicolás, I. Navarro-Blasco, J.M. Fernández, J.I. Alvarez, Atmospheric NOx removal: study of cement mortars with iron-and vanadium-doped TiO2 as visible light - sensitive photocatalysts, Construction and Building Materials 149 (2017) 257-271.

[10] A. Gandolfo, V. Bartolomei, E.G. Alvarez, S. Tlili, S. Gligorovski, J. Kleffmann, H. Wortham, The effectiveness of indoor photocatalytic paints on NOx and HONO levels, Applied Catalysis B: Environmental 166 (2015) 84-90.

[11] J. Patzsch, A. Folli, D.E. Macphee, J.Z. Bloh, On the underlying mechanisms of the low observed

nitrate selectivity in photocatalytic NO x abatement and the importance of the oxygen reduction reaction, Physical Chemistry Chemical Physics 19(48) (2017) 32678-32686.
[12] S. Jin, G. Dong, J. Luo, F. Ma, C. Wang, Improved photocatalytic NO removal activity of SrTiO3 by using SrCO3 as a new co-catalyst, Applied Catalysis B: Environmental 227 (2018) 24-34.
[13] J. Zhao, X. Yang, Photocatalytic oxidation for indoor air purification: a literature review, Building and Environment 38(5) (2003) 645-654.
[14] F. Gauvin, V. Caprai, Q. Yu, H. Brouwers, Effect of the morphology and pore structure of porous building materials on photocatalytic oxidation of air pollutants, Applied Catalysis B: Environmental 227 (2018) 123-131.
[15] D. Fan, C. Guo, H. Ma, D. Zhao, Y. Li, D. Wu, Q. Wei, Facile fabrication of an aptasensor for thrombin based on graphitic carbon nitride/TiO2 with high visible-light photoelectrochemical activity, Biosensors and Bioelectronics 75 (2016) 116-122.
[16] Y. Ling, G. Liao, Y. Xie, J. Yin, J. Huang, W. Feng, L. Li, Coupling photocatalysis with ozonation for enhanced degradation of Atenolol by Ag-TiO2 micro-tube, Journal of Photochemistry and Photobiology A: Chemistry 329 (2016) 280-286.
[17] T. Yang, J. Peng, Y. Zheng, X. He, Y. Hou, L. Wu, X. Fu, Enhanced photocatalytic ozonation degradation of organic pollutants by ZnO modified TiO2 nanocomposites, Applied Catalysis B: Environmental 221 (2018) 223-234.
[18] W.-J. Ong, L.-L. Tan, Y.H. Ng, S.-T. Yong, S.-P. Chai, Graphitic carbon nitride (g-C3N4)-based photocatalysts for artificial photosynthesis and environmental remediation: are we a step closer to achieving sustainability?, Chemical reviews 116(12) (2016) 7159-7329.
[19] X. Lu, K. Xu, P. Chen, K. Jia, S. Liu, C. Wu, Facile one step method realizing scalable production of gC 3 N 4 nanosheets and study of their photocatalytic H 2 evolution activity, Journal of materials chemistry A 2(44) (2014) 18924-18928.
[20] J. Wen, J. Xie, X. Chen, X. Li, A review on g-C3N4-based photocatalysts, Applied surface science 391 (2017) 72-123.
[21] G. Mamba, A. Mishra, Graphitic carbon nitride (g-C3N4) nanocomposites: a new and exciting generation of visible light driven photocatalysts for environmental pollution remediation, Applied Catalysis B: Environmental 198 (2016) 347-377.
[22] I. Papailias, T. Giannakopoulou, N. Todorova, D. Demotikali, T. Vaimakis, C. Trapalis, Effect of processing temperature on structure and photocatalytic properties of g-C3N4, Applied Surface Science 358 (2015) 278-286.
[23] Y. Yang, T. Ji, W. Su, B. Yang, Y. Zhang, Z. Yang, Photocatalytic NOx abatement and self-cleaning performance of cementitious composites with g-C3N4 nanosheets under visible light, Construction and Building Materials 225 (2019) 120-131.
[24] F. Peng, Y. Ni, Q. Zhou, J. Kou, C. Lu, Z. Xu, New g-C3N4 based photocatalytic cement with enhanced visible-light photocatalytic activity by constructing muscovite sheet/SnO2 structures, Construction and Building Materials 179 (2018) 315-325.
[25] M. Pérez-Nicolás, J. Balbuena, M. Cruz-Yusta, L. Sánchez, I. Navarro-Blasco, J. Fernández, J. Alvarez, Photocatalytic NOx abatement by calcium aluminate cements modified with TiO2: Improved NO2 conversion, Cement and Concrete Research 70 (2015) 67-76.
[26] M.-Z. Guo, T.-C. Ling, C.S. Poon, Photocatalytic NOx degradation of concrete surface layers intermixed and spray-coated with nano-TiO2: Influence of experimental factors, Cement and Concrete Composites 83 (2017) 279-289.
[27] M. Faraldos, R. Kropp, M. Anderson, K. Sobolev, Photocatalytic hydrophobic concrete coatings to combat air pollution, Catalysis Today 259 (2016) 228-236.

[28] M. Lettieri, D. Colangiuli, M. Masieri, A. Calia, Field performances of nanosized TiO2 coated limestone for a self-cleaning building surface in an urban environment, Building and Environment 147 (2019) 506-516.
[29] Q. Li, Q. Liu, B. Peng, L. Chai, H. Liu, Self-cleaning performance of TiO2-coating cement materials prepared based on solidification/stabilization of electrolytic manganese residue, Construction and Building Materials 106 (2016) 236-242.
[30] B. Jalvo, M. Faraldos, A. Bahamonde, R. Rosal, Antibacterial surfaces prepared by electrospray coating of photocatalytic nanoparticles, Chemical Engineering Journal 334 (2018) 1108-1118.
[31] (!!! INVALID CITATION !!! [31-33]).
[32] M.-Z. Guo, J. Chen, M. Xia, T. Wang, C.S. Poon, Pathways of conversion of nitrogen oxides by nano TiO2 incorporated in cement-based materials, Building and Environment 144 (2018) 412-418.
[33] M.M. Hassan, H. Dylla, L.N. Mohammad, T. Rupnow, Evaluation of the durability of titanium dioxide photocatalyst coating for concrete pavement, Construction and building materials 24(8) (2010) 1456-1461.
[34] N. Bossa, P. Chaurand, C. Levard, D. Borschneck, H. Miche, J. Vicente, C. Geantet, O. Aguerre-Chariol, F.M. Michel, J. Rose, Environmental exposure to TiO2 nanomaterials incorporated in building material, Environmental pollution 220 (2017) 1160-1170.
[35] S.A. Diamond, A.J. Kennedy, N.L. Melby, R.D. Moser, A. Poda, C. Weiss Jr, J. Brame, Assessment of the potential hazard of nano-scale TiO2 in photocatalytic cement: application of a tiered assessment framework, NanoImpact 8 (2017) 11-19.
[36] A. Maury-Ramirez, K. Demeestere, N. De Belie, Photocatalytic activity of titanium dioxide nanoparticle coatings applied on autoclaved aerated concrete: effect of weathering on coating physical characteristics and gaseous toluene removal, Journal of hazardous materials 211 (2012) 218-225.
[37] A.M. Ramirez, K. Demeestere, N. De Belie, T. Mäntylä, E. Levänen, Titanium dioxide coated cementitious materials for air purifying purposes: preparation, characterization and toluene removal potential, Building and Environment 45(4) (2010) 832-838.
[38] J. Olabarrieta, S. Zorita, I. Peña, N. Rioja, O. Monzón, P. Benguria, L. Scifo, Aging of photocatalytic coatings under a water flow: long run performance and TiO2 nanoparticles release, Applied Catalysis B: Environmental 123 (2012) 182-192.
[39] D.B. Warheit, C.M. Sayes, K.L. Reed, K.A. Swain, Health effects related to nanoparticle exposures: environmental, health and safety considerations for assessing hazards and risks, Pharmacology & therapeutics 120(1) (2008) 35-42.
[40] K. Inoue, H. Takano, M. Ohnuki, R. Yanagisawa, M. Sakurai, A. Shimada, K. Mizushima, T. Yoshikawa, Size effects of nanomaterials on lung inflammation and coagulatory disturbance, International journal of immunopathology and pharmacology 21(1) (2008) 197-206.
[41] T. Verdier, A. Bertron, B. Erable, C. Roques, Bacterial biofilm characterization and microscopic evaluation of the antibacterial properties of a photocatalytic coating protecting building material, Coatings 8(3) (2018) 93.
[42] S.S. Alias, Z. Harun, I.S.A. Latif, Characterization and performance of porous photocatalytic ceramic membranes coated with Ti0 2 via different dip-coating routes, Journal of materials science 53(16) (2018) 11534-11552.
[43] D. Colangiuli, A. Calia, N. Bianco, Novel multifunctional coatings with photocatalytic and hydrophobic properties for the preservation of the stone building heritage, Construction and Building Materials 93 (2015) 189-196.
[44] (!!! INVALID CITATION !!! [46-48]).
[45] M.F. La Russa, N. Rovella, M.A. de Buergo, C.M. Belfiore, A. Pezzino, G.M. Crisci, S.A. Ruffolo,

Nano-TiO2 coatings for cultural heritage protection: The role of the binder on hydrophobic and self-cleaning efficacy, Progress in Organic Coatings 91 (2016) 1-8.
[46] M.F. La Russa, S.A. Ruffolo, N. Rovella, C.M. Belfiore, A.M. Palermo, M.T. Guzzi, G.M. Crisci, Multifunctional TiO2 coatings for cultural heritage, Progress in Organic Coatings 74(1) (2012) 186-191.
[47] F. Persico, M. Sansotera, C.L. Bianchi, C. Cavallotti, W. Navarrini, Photocatalytic activity of TiO2-embedded fluorinated transparent coating for oxidation of hydrosoluble pollutants in turbid suspensions, Applied Catalysis B: Environmental 170 (2015) 83-89.
[48] C. Mendoza, A. Valle, M. Castellote, A. Bahamonde, M. Faraldos, TiO2 and TiO2 - SiO2 coated cement: Comparison of mechanic and photocatalytic properties, Applied Catalysis B: Environmental 178 (2015) 155-164.
[49] F. Pino, P. Fermo, M. La Russa, S. Ruffolo, V. Comite, J. Baghdachi, E. Pecchioni, F. Fratini, G. Cappelletti, Advanced mortar coatings for cultural heritage protection. Durability towards prolonged UV and outdoor exposure, Environmental Science and Pollution Research 24(14) (2017) 12608-12617.
[50] P. Carmona-Quiroga, S. Martínez-Ramírez, H. Viles, Efficiency and durability of a self-cleaning coating on concrete and stones under both natural and artificial ageing trials, Applied Surface Science 433 (2018) 312-320.
[51] Y. Zhang, J. Liu, G. Wu, W. Chen, Porous graphitic carbon nitride synthesized via direct polymerization of urea for efficient sunlight-driven photocatalytic hydrogen production, Nanoscale 4(17) (2012) 5300-5303.
[52] M. Drdácký, J. Lesák, S. Rescic, Z. Slí ková, P. Tiano, J. Valach, Standardization of peeling tests for assessing the cohesion and consolidation characteristics of historic stone surfaces, Materials and structures 45(4) (2012) 505-520.
[53] A. Calia, M. Lettieri, M. Masieri, Durability assessment of nanostructured TiO2 coatings applied on limestones to enhance building surface with self-cleaning ability, Building and Environment 110 (2016) 1-10.
[54] M.-Z. Guo, J.-S. Li, C.S. Poon, Improved photocatalytic nitrogen oxides removal using recycled glass-nano-TiO2 composites with NaOH pre-treatment, Journal of Cleaner Production 209 (2019) 1095-1104.
[55] V.K. Yemmireddy, G.D. Farrell, Y.C. Hung, Development of titanium dioxide (TiO2) nanocoatings on food contact surfaces and method to evaluate their durability and photocatalytic bactericidal property, Journal of food science 80(8) (2015) N1903-N1911.
[56] D. Colangiuli, M. Lettieri, M. Masieri, A. Calia, Field study in an urban environment of simultaneous self-cleaning and hydrophobic nanosized TiO2-based coatings on stone for the protection of building surface, Science of The Total Environment 650 (2019) 2919-2930.
[57] I. Alfieri, A. Lorenzi, L. Ranzenigo, L. Lazzarini, G. Predieri, P.P. Lottici, Synthesis and characterization of photocatalytic hydrophobic hybrid TiO2-SiO2 coatings for building applications, Building and Environment 111 (2017) 72-79.
[58] G. Jiang, J. Cao, M. Chen, X. Zhang, F. Dong, Photocatalytic NO oxidation on N-doped TiO2/g-C3N4 heterojunction: Enhanced efficiency, mechanism and reaction pathway, Applied Surface Science 458 (2018) 77-85.
[59] T. Martinez, A. Bertron, E. Ringot, G. Escadeillas, Degradation of NO using photocatalytic coatings applied to different substrates, Building and Environment 46(9) (2011) 1808-1816.
[60] P. Munafo, G.B. Goffredo, E. Quagliarini, TiO2-based nanocoatings for preserving architectural stone surfaces: An overview, Construction and Building materials 84 (2015) 201-218.

[61] M.V. Diamanti, R. Paolini, M. Rossini, A.B. Aslan, M. Zinzi, T. Poli, M.P. Pedeferri, Long term self-cleaning and photocatalytic performance of anatase added mortars exposed to the urban environment, Construction and Building Materials 96 (2015) 270-278.
[62] C. Sciancalepore, F. Bondioli, Durability of SiO2 - TiO2 photocatalytic coatings on ceramic tiles, International Journal of Applied Ceramic Technology 12(3) (2015) 679-684.
[63] P. Krishnan, M.-H. Zhang, L. Yu, H. Feng, Photocatalytic degradation of particulate pollutants and self-cleaning performance of TiO2-containing silicate coating and mortar, Construction and Building Materials 44 (2013) 309-316.
[64] R. Paolini, M. Sleiman, M. Pedeferri, M.V. Diamanti, TiO2 alterations with natural aging: Unveiling the role of nitric acid on NIR reflectance, Solar Energy Materials and Solar Cells 157 (2016) 791-797.
[65] H. Che, L. Liu, G. Che, H. Dong, C. Liu, C. Li, Control of energy band, layer structure and vacancy defect of graphitic carbon nitride by intercalated hydrogen bond effect of NO3- toward improving photocatalytic performance, Chemical Engineering Journal 357 (2019) 209-219.
[66] Y. Li, Y. Sun, W. Ho, Y. Zhang, H. Huang, Q. Cai, F. Dong, Highly enhanced visible-light photocatalytic NOx purification and conversion pathway on self-structurally modified g-C3N4 nanosheets, Science Bulletin 63(10) (2018) 609-620.